PERGAMON

Journal of Structural Geology 25 (2003) 1083–1096

JOURNAL OF STRUCTURAL GEOLOGY

www.elsevier.com/locate/jsg

Rotation of long tectonic clasts in transpressional shear zones

S.K. Ghosh[a,*], G. Sen[b], S. Sengupta[a]

[a]*Department of Geological Sciences, Jadavpur University, Calcutta 700 032, India*
[b]*School of Oceanographic Studies, Jadavpur University, Calcutta 700 032, India*

Received 16 December 2001; received in revised form 24 July 2002; accepted 29 July 2002

Abstract

The two-dimensional analysis of rotation of rigid ellipsoidal inclusions is not applicable to situations in which either the bulk deformation deviates from plane-strain or one of the principal axes of the inclusion is at an angle to the vorticity vector. Both these situations may occur in certain types of transpressional ductile shear zones. The model presented here shows how long cylindrical or ellipsoidal tectonic clasts (with the longest axis parallel to the walls of the shear zone but at an angle to the vorticity vector) rotate in transpressional shear zones. Long clasts, initially at a low angle to the vorticity vector and at a large angle to the stretching lineation, will rotate and tend to become subparallel to the stretching lineation. The rotation of the principal axes of the elliptical cross-section around the cylinder axis cannot be unlimited for any inclusion, including the inclusion with circular cross-section ($R = 1$); if the deformation is sufficiently large there is always a stable position of orientation. The model explains simultaneous occurrence of monoclinic rolling structures in sections parallel and perpendicular to the vorticity vector. Depending upon the initial orientation, the long axes of different clasts in the foliation plane may rotate clockwise and counterclockwise. Consequently, opposite senses of asymmetry of rolling structures may appear in sections parallel to the vorticity vector.

Keywords: Rotation of clasts; Transpression; Stretching lineation

1. Introduction

Ghosh and Ramberg (1976) had considered rotation of elongate inclusions in combined pure shear and simple shear. This model has been applied to many geological situations to interpret structures resulting from rotation of porphyroclasts, porphyroblasts and boudins (e.g. Ghosh, 1977; Passchier and Simpson, 1986; Passchier, 1987; Simpson and De Paor, 1997). The application of this model is justified when one of the principal axes of the inclusion is parallel to the vorticity vector.

As pointed out by Passchier and Trouw (1996, p. 106), many mylonites show a clear difference in structures in sections normal and parallel to the stretching lineation, with monoclinic rolling structures (Van Den Driessche and Brun, 1987) appearing in sections parallel to the stretching lineation and normal to the vorticity vector, and with orthorhombic structures appearing in sections normal to the lineation and parallel to the vorticity vector. On the other hand, stretching lineations parallel to the vorticity vector have also been reported from some transpressional shear zones (e.g. Hudleston et al., 1988; Tikoff and Greene, 1997). For such shear zones the monoclinic structures are seen in sections normal to the stretching lineation. The problem considered in this paper arose from our studies in the Phulad shear zone (Ghosh et al., 1999) of Rajasthan, India, where the steep stretching lineation is perpendicular to the subhorizontal vorticity vector, and yet, monoclinic structures around long tectonic clasts are often seen in subhorizontal sections normal to the stretching lineation and subparallel to the vorticity vector. In the following sections we present a model that explains simultaneous occurrence of monoclinic structures in sections both parallel and perpendicular to the vorticity vector.

We consider below the rotational behaviour of rigid long cylindrical bodies (e.g. long cylindroidal clasts, rodding, boudins with length much greater along the boudin axes than along cross-sections), embedded in a viscous matrix, with their long axis in a plane parallel to the walls of a shear zone undergoing three-dimensional noncoaxial deformation. It is assumed that the cylindrical body has an elliptical cross-section and the cylinder axis is at an angle to the vorticity vector. The model is also applicable to

* Corresponding author.
E-mail address: subir30@hotmail.com (S.K. Ghosh).

0191-8141/03/$ - see front matter © 2002 Elsevier Science Ltd. All rights reserved.
PII: S0191-8141(02)00146-3

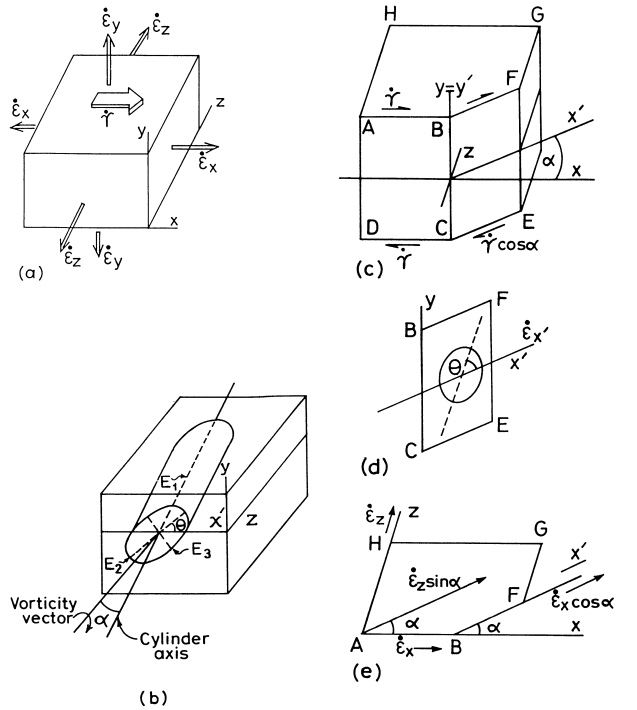

Fig. 1. (a) Nature of bulk deformation in a transpressional ductile shear zone. The shear zone walls are parallel to the xz co-ordinate plane. The bulk instantaneous deformation is by a combination of simple shear (with strain rate $\dot{\gamma}$) and three-dimensional coaxial deformation (with strain rates $\dot{\epsilon}_x$, $\dot{\epsilon}_y$ and $\dot{\epsilon}_z$). (b) Long cylindrical clast with axis at an angle with the vorticity vector. The vorticity vector is parallel to the z co-ordinate axis. The axis of the cylinder E_1 lies on the xz plane but makes an angle α with the vorticity vector (parallel to the z co-ordinate axis). The elliptical cross-section has principal axes E_2 and E_3 with $E_2 > E_3$. E_2 makes an angle of θ with the x' co-ordinate axis. (c) BFEC is a plane parallel to the cross-section of an elliptical cylinder, the axis of which is normal to this plane. The x' axis is parallel to the trace of the xz co-ordinate plane on the cross-sectional plane BFEC. The angle between the x' and x axes is α. The component of simple shear strain rate along x' is $\dot{\gamma}\cos\alpha$. (d) For the case of $\alpha \neq 0$, the angle between the x' axis and the major axis of the elliptical cross-section is θ. The component of $\dot{\epsilon}_x$ along x' is $\dot{\epsilon}_{x'}$. (e) The plane ABFGH of (c). Along the x' direction the component of $\dot{\epsilon}_z$ is $\dot{\epsilon}_z\sin\alpha$.

ellipsoidal inclusions in which one of the principal axes is much longer than the other two. In such a situation, rotation of the major axis of the elliptical cross-section about the cylinder axis will be associated with rotation of the cylinder axis itself within a plane parallel to the shear zone walls.

This is not a general model for rotation of inclusions in ductile shear zones because the deformation in the shear zone, unlike the model considered by Robin and Cruden (1994), has been taken to be homogeneous. Moreover, we are also considering a special case in which the long axes of the cylindrical clasts are assumed to be parallel to the mylonitic foliation. As was evident from our field studies in the Phulad shear zone, this latter assumption is justified for certain types of long clasts such as boudins, detached fold hinges and rodding structures or long cylindroidal bodies of pegmatite that remain parallel to the mylonitic foliation.

2. Nature of bulk deformation

We are considering a three-dimensional noncoaxial deformation in a tabular zone (Fig. 1a). Let the y co-ordinate axis be perpendicular to the shear zone walls, and let the x and z axes be parallel to the walls, with the x axis parallel to the direction of simple shearing and the z axis parallel to the vorticity vector. The deformation is obtained by simultaneous superposition of simple shearing with strain rate $\dot{\gamma}(=\dot{\gamma}_{xy})$ and three-dimensional noncoaxial deformation with strain rates $\dot{\epsilon}_x$, $\dot{\epsilon}_y$ and $\dot{\epsilon}_z$ (Fig. 1a). For such a deformation, if $\dot{\epsilon}_x \neq \dot{\epsilon}_y$, a point (x_o, y_o, z_o) changes to a point (x, y, z) according to the equations:

$$x = e^{a\gamma}x_o + \left(e^{b\gamma} - e^{a\gamma}\right)y_o/(b-a),$$

$$y = e^{b\gamma}y_o,$$

$$z = e^{c\gamma}z_o = (e^{-(a+b)\gamma})z_o, \tag{1}$$

where

$$a = \dot{\epsilon}_x/\dot{\gamma},\ b = \dot{\epsilon}_y/\dot{\gamma},\ c = \dot{\epsilon}_z/\dot{\gamma}, \tag{2}$$

and where, for constant-volume deformation:

$$\dot{\epsilon}_x + \dot{\epsilon}_y + \dot{\epsilon}_z = 0 \text{ or } a + b + c = 0,$$

(Ghosh, 2001). Depending on whether b in Eq. (1) is negative or positive, the deformation in the tabular zone will be transpressional or transtensional. In the following analysis, we shall be concerned with transpressional deformation. Hence, unless specified otherwise, $\dot{\epsilon}_y$ or b will be negative or contractional.

3. Rotation of a cylindrical inclusion with elliptical cross-section, the cylinder axis lying in the shear plane but making an angle with the vorticity vector

We are considering the rotation of an embedded object or inclusion that is either a cylinder with elliptical cross-section or is an ellipsoid in which one of the principal axes is much larger than the other two. The cylinder axis or the longest axis of the ellipsoid will be called E_1, whereas the major and the minor axes of the cross-sectional ellipse will be called E_2 and E_3 (Fig. 1b), with $E_2 > E_3$ and with the cross-sectional aspect ratio $R = E_2/E_3$. It is assumed that the cylinder axis E_1 lies in the xz co-ordinate plane, i.e. the plane containing the direction of simple shear (x-axis) and the vorticity vector (z-axis). The E_1 axis makes an angle α with the z co-ordinate axis (Fig.1b and c). In Fig.1c, ABCD is a plane perpendicular to the vorticity vector (i.e. parallel to the xy plane). BCEF is a plane perpendicular to E_1. The trace of the xz plane on the BCEF plane is the x' axis. The angle between the x and x' axes is α (Fig. 1c and d). The major axis of the elliptical cross-section of the cylinder makes an angle θ with the x' axis (Fig. 1d). On

the cross-sectional plane, the y' axis is perpendicular to the x' axis, and thus y' remains parallel to y. Since the x' axis is at an angle to the x and z axes (Fig. 1e), the strain rate parallel to the x' axis is:

$$\dot{\epsilon}_{x'} = \dot{\epsilon}_x \cos\alpha + \dot{\epsilon}_z \sin\alpha. \tag{3}$$

The component of simple shear strain rate on the $x'y'$ plane is:

$$\dot{\gamma}_{(a)} = \dot{\gamma}\cos\alpha. \tag{4}$$

Because of the component of simple shear $\dot{\gamma}_{(a)}$, the rate of rotation of the elliptical cross-section around the cylinder axis will be, from Ghosh and Ramberg (1976):

$$-\dot{\theta}_\gamma = \dot{\gamma}\cos\alpha\left(R^2\sin^2\theta + \cos^2\theta\right)\left(\frac{1}{R^2+1}\right). \tag{5}$$

Because of the strain-rate $\dot{\epsilon}_{x'}$ the rate of rotation will be (Ghosh and Sengupta, 1973; Ghosh and Ramberg, 1976, p. 4):

$$-\dot{\theta}_\epsilon(1) = \frac{1}{2}\dot{\epsilon}_{x'}\left(\frac{R^2-1}{R^2+1}\right)\sin 2\theta. \tag{6}$$

From Eqs. (3) and (6), we have:

$$-\dot{\theta}_\epsilon(1) = \frac{1}{2}\left(\dot{\epsilon}_x\cos\alpha + \dot{\epsilon}_z\sin\alpha\right)\left(\frac{R^2-1}{R^2+1}\right)\sin 2\theta. \tag{7}$$

This is the rotation rate of the inclusion for $\dot{\epsilon}_{x'}$ alone.

The rotation rate resulting from $\dot{\epsilon}_y$ is:

$$-\dot{\theta}_\epsilon(2) = -\frac{1}{2}\dot{\epsilon}_y\left(\frac{R^2-1}{R^2+1}\right)\sin 2\theta. \tag{8}$$

The total rotation rate is the sum of all these:

$$\dot{\theta} = \dot{\theta}_y + \dot{\theta}_\epsilon(1) + \dot{\theta}_\epsilon(2), \tag{9}$$

$$\begin{aligned}\frac{-\dot{\theta}}{\dot{\gamma}} &= \left(\frac{R^2}{R^2+1}\right)\cos\alpha\sin^2\theta + \left(\frac{1}{R^2+1}\right)\cos\alpha\cos^2\theta \\ &\quad + \frac{1}{2}\left[\left(\frac{\dot{\epsilon}_x}{\dot{\gamma}}\right)\cos\alpha - \left(\frac{\dot{\epsilon}_y}{\dot{\gamma}}\right) + \left(\frac{\dot{\epsilon}_z}{\dot{\gamma}}\right)\sin\alpha\right] \\ &\quad \times\left(\frac{R^2-1}{R^2+1}\right)\sin 2\theta.\end{aligned} \tag{10}$$

With a, b and c as given by Eq. (2), Eq. (10) can be written as:

$$\frac{-\dot{\theta}}{\dot{\gamma}} = A\sin^2\theta + B\sin 2\theta + C\cos^2\theta, \tag{11}$$

where

$$A = \left(\frac{R^2}{R^2+1}\right)\cos\alpha,$$

$$B = \frac{1}{2}(a\cos\alpha - b + c\sin\alpha)\left(\frac{R^2-1}{R^2+1}\right),$$

$$C = \left(\frac{1}{R^2+1}\right)\cos\alpha. \tag{12}$$

The rate of rotation of a passive marker is obtained when $R = \infty$. In practice, the rate of rotation of a passive marker can be obtained by taking a sufficiently large value of R. Thus, for example, if the aspect ratio is 10, the maximum difference in its rate of rotation from that of a passive marker is $<1°$. If the aspect ratio is six, this difference is $<2°$.

In the course of deformation, the angle α that the E_1 axis makes with the z axis will also change. Since E_1 is assumed to be sufficiently long (with $E_1/E_2 > 6$) it has been assumed that it will rotate essentially as a marker line. For finite deformation, a material particle with initial position (x_o, y_o, z_o), will change to the position (x, y, z):

$$x = e^{a\gamma}x_o + \left[\frac{(e^{b\gamma} - e^{a\gamma})}{(b-a)}\right]y_o,$$

$$y = e^{b\gamma}y_o,$$

$$z = e^{-(a+b)\gamma}z_o$$

(Ghosh, 2001, eqs. 22–24). On the xz plane, $y = 0$:

$$\tan\alpha = x/z = e^{(a-c)\gamma}\tan\alpha_o. \tag{13}$$

Eq. (13) shows that, for a given initial angle α_o, the angle α will increase with progressive deformation. An increase in α means that the cylinder axis rotates away from the z-axis and towards the x-axis. As the deformation becomes very large, α tends to 90° and the rotation around the cylinder axis becomes increasingly small. Eq. (13) also shows that the sense of rotation of the E_1 axis is reversed if the sign of α_o is reversed. Eqs. (11)–(13) show that when $\alpha \neq 0$, the rate of rotation of the inclusion around the cylinder axis is a function of both θ and α. For given initial values of θ_o and α_o, both θ and α will change with progressive deformation. At each stage, the rotation around the cylinder axis is $\omega = \theta - \theta_o$.

A, B and C, as given by Eq. (12), do not remain constant but are functions of α, and change with progressive deformation as α increases. If $\Delta\gamma$ is taken in small increments, the incremental form of Eq. (11) can be written as:

$$\Delta\theta = \Delta\gamma\left(A\sin^2\theta + B\sin 2\theta + C\cos^2\theta\right). \tag{14}$$

For given θ_o and α_o, $\Delta\theta$ is calculated from Eq. (14) for a small increment $\Delta\gamma$. After each increment the new value of θ is obtained by adding $\Delta\theta$ to the earlier value of θ. The new value of α is obtained from Eq. (13). The new values of A, B and C are determined from Eq. (12) and the process is repeated. In the numerical calculations γ was increased by 0.01, and θ of successive stages was determined up to $\gamma = 100$.

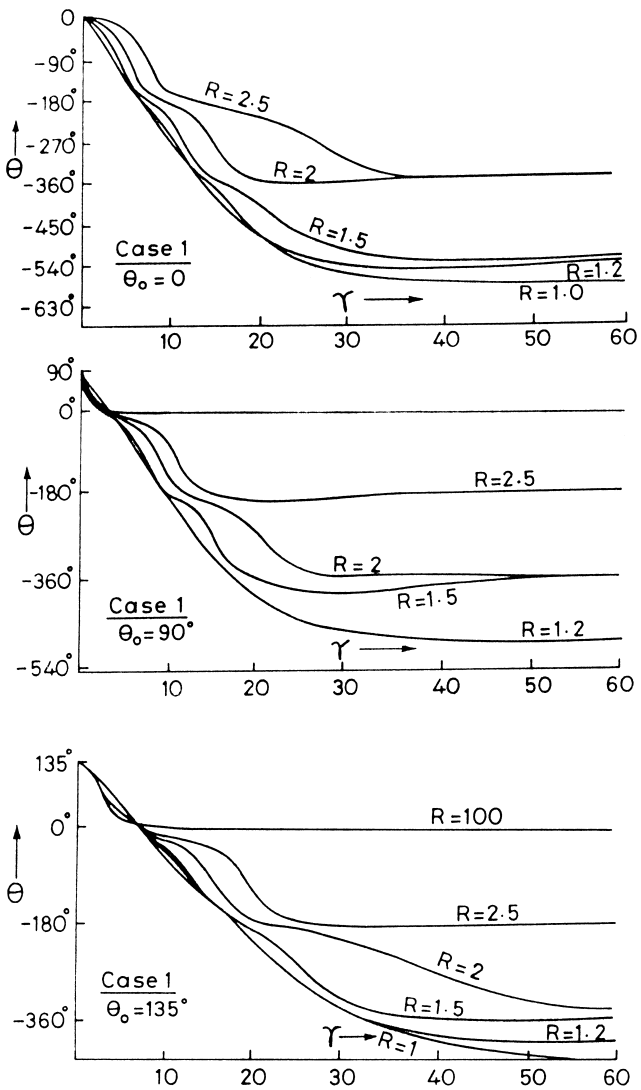

Fig. 2. Finite rotation of long clasts with $\alpha_o = 5°$, for case 1 ($a = 0.2$, $b = -0.25$, $c = 0.05$) with (a) $\theta_o = 0$, (b) $\theta_o = 90°$ and (c) $\theta_o = 135°$.

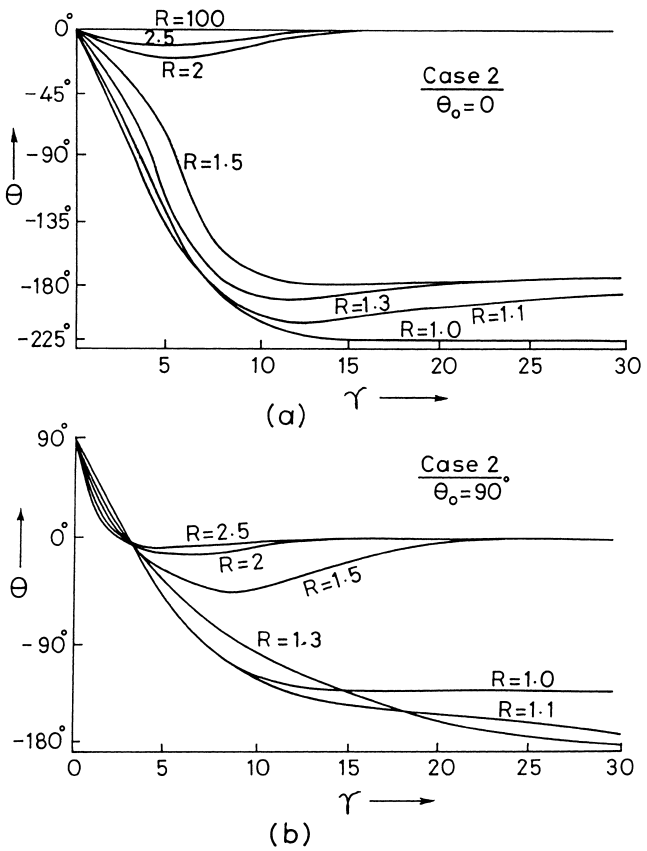

Fig. 3. Finite rotation of long clasts with $\alpha_o = 5°$, for case 2 ($a = 0.5$, $b = -0.6$, $c = 0.1$) for (a) $\theta_o = 0$ and (b) $\theta_o = 90°$.

4. Examples of rates of rotation and of finite rotation of inclusions for $\alpha \neq 0$

We have chosen four cases of bulk deformation with four sets of strain-rate ratios:

case 1: $a = 0.2$, $b = -0.25$, $c = 0.05$;
case 2: $a = 0.5$, $b = -0.6$, $c = 0.1$;
case 3: $a = 0.8$, $b = -1.0$, $c = 0.2$;
case 4: $a = 1.5$, $b = -2.0$, $c = 0.5$.
$\alpha_o = 5°$ for all the cases.

All of these are examples of transpressional deformation with stretching along the direction of simple shearing as well as along the direction of the vorticity vector. The stretching rate along the direction of simple shearing (x co-ordinate axis) is greater than along the vorticity vector (z co-ordinate axis). From example 1 to example 4, the value of a ($= \dot{\epsilon_x}/\dot{\gamma}$) increases or, in other words, the relative contribution of simple shearing with respect to coaxial straining decreases. We shall consider the rotation of inclusions with different aspect ratios ($R = E_2/E_3$) in each of these four types of deformation.

If $\alpha = 0$, an inclusion can either rotate forward or it can rotate backward, but the sense of rotation is never reversed during progressive deformation. Moreover, in this case, inclusions with relatively small values of R ($R < R_c$) may undergo unlimited forward rotation with progressive deformation (Ghosh and Ramberg, 1976). In contrast, for the case of $\alpha \neq 0$, the rotation cannot be unlimited for any inclusion, including the inclusion with circular cross-section ($R = 1$); if the deformation is sufficiently large there is always a stable position of orientation.

In general, we may have three types of curves for finite rotation (Figs. 2–5): (i) curves that show at first a relatively small (an acute angle) forward rotation and then the same amount of backward rotation so that the inclusion may be finally stabilised at $\theta = 0$ (e.g. curves for $R = 1.62$ and $R = 2$ in Fig. 4a); (ii) curves that show a forward rotation through more that 180° (or a multiple of 180°) and then backward rotation through an

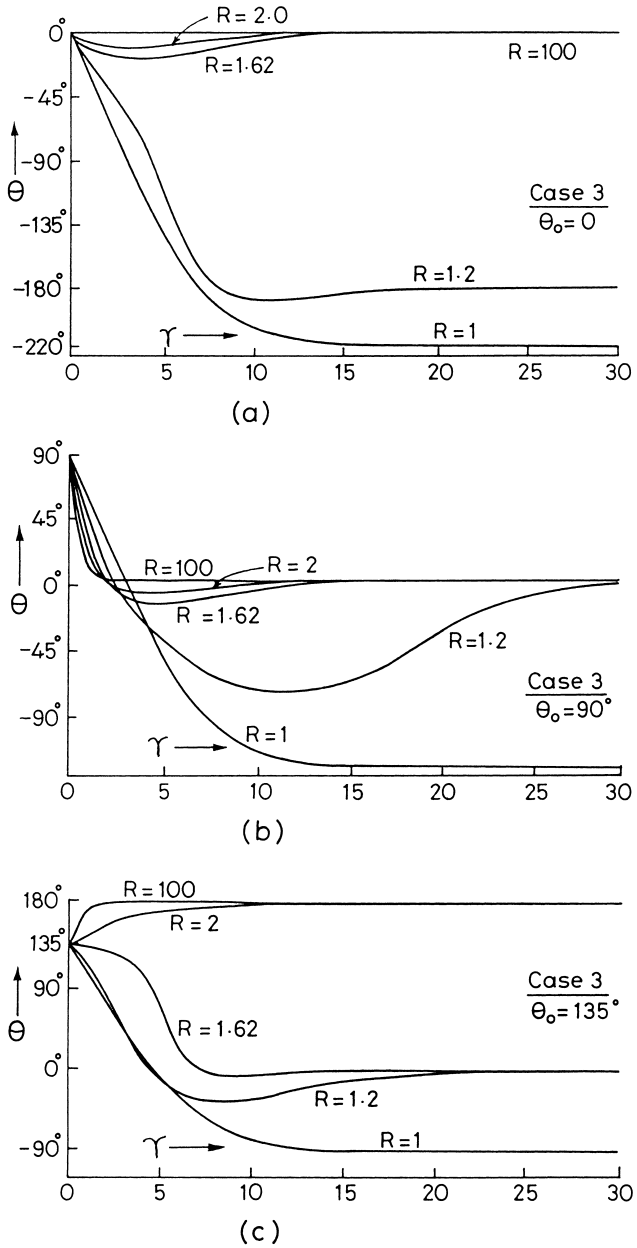

Fig. 4. Finite rotation of long clasts with $\alpha_o = 5°$ for case 3 ($a = 0.8$, $b = -1.0$, $c = 0.2$) for (a) $\theta_o = 0$, (b) $\theta_o = 90°$ and (c) $\theta_o = 135°$.

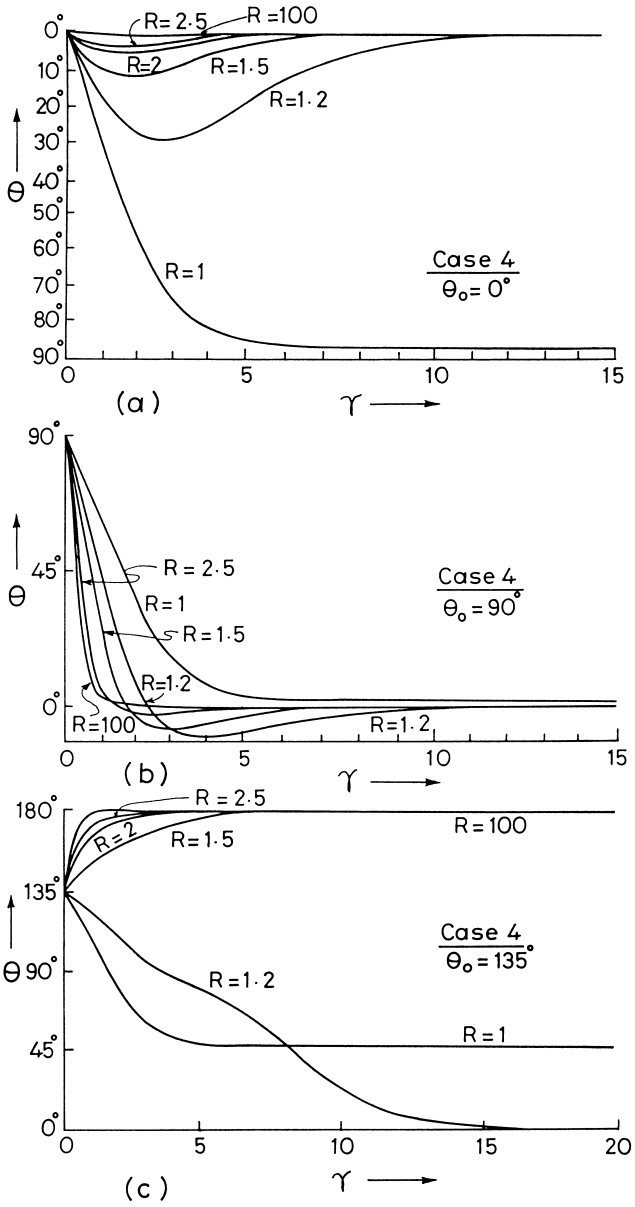

Fig. 5. Finite rotation of long clasts with $\alpha_o = 5°$ for case 4 ($a = 1.5$, $b = -2.0$, $c = 0.5$) for (a) $\theta_o = 0$, (b) $\theta_o = 90°$ and (c) $\theta_o = 135°$.

acute angle, to be stabilised at 180° (or a multiple of 180°) (e.g. the curve for $R = 1.2$ in Fig. 4a); and (iii) curves that show only a forward rotation and a stable position at 180° or a multiple of 180° (e.g. the curve for $R = 1.1$ in Fig. 3b). An inclusion with a circular cross-section can only rotate forward. Although the concept of a stable orientation is inapplicable for circular sections, the curves for finite deformation (θ versus γ curves) become parallel to the γ axis. Thus, the forward rotation of an inclusion with $R = 1$ approaches a limiting value similar to inclusions with $R > 1$. However, for inclusions with $R = 1$, this limiting value is not necessarily a multiple of 180°.

5. Stable orientation, critical value of R, forward and backward rotation when $\alpha \neq 0$

5.1. Critical value of R

Unlike the special case of $\alpha = 0$ (Ghosh and Ramberg, 1976), there is, for the case of $\alpha \neq 0$, no fixed critical value of R that separates inclusions that may undergo only forward rotation from those that may rotate backward at certain orientations. For $\alpha \neq 0$, the critical value R (R_c) is:

$$R_c = (1/2F)[1 + (1 + 4F^2)^{1/2}], \quad (15)$$

where $F = (1/2\cos\alpha)(a\cos\alpha - b + c\sin\alpha)$.

Among the critical orientations considered by Ghosh and Ramberg (1976), the orientation that is relevant for us is θ_5.

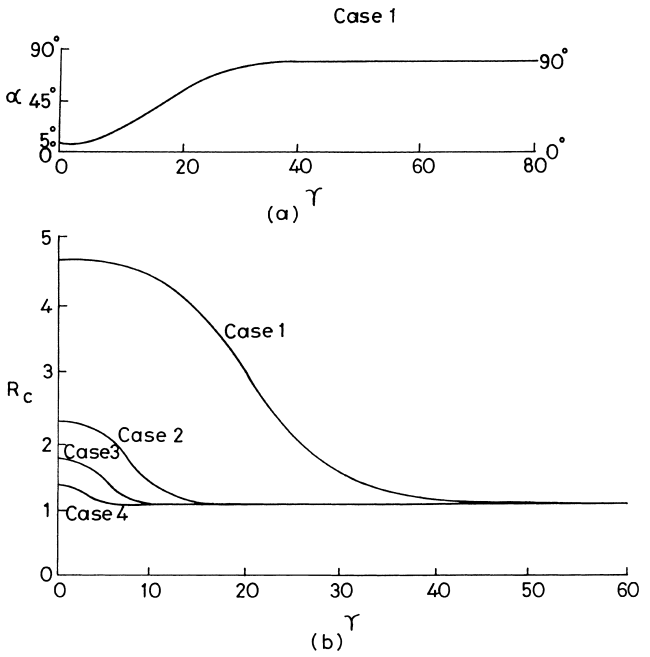

Fig. 6. (a) Change in α with progressive deformation in case 1, with $\alpha_o = 5°$. With increasing deformation α tends to be 90° as the E_1 axis tends to become parallel to the x-axis. (b) Change in the critical value R_c with progressive deformation. At a large value of deformation R_c tends to become one.

This orientation is obtained by putting $\dot{\theta}/\dot{\gamma} = 0$ in Eq. (11):

$$\tan\theta_5 = [-B + (B^2 - AC)^{1/2}]/A \quad (16)$$

where A, B and C are given by Eq. (12).

The critical value of R is a function of α and the strain-rate ratios of bulk deformation a, b and c (Fig. 6b). It is independent of θ_o and R. The rotation of the inclusion will be in the forward sense when $R < R_c$. Backward rotation may occur if $R > R_c$. Moreover, as shown by Eq. (12), the parameters A, B and C, being functions of α and R, change with progressive deformation. Hence, the orientations at which the rate of rotation becomes zero will also depend on these parameters.

Eq. (15) shows that R_c is independent of R and θ_o. For any set of a, b, c and initial α, R_c decreases with progressive deformation. At the beginning of deformation, for an inclusion with aspect ratio R and initial orientation θ_o, the initial R_c (i.e. the value of R_c at the beginning of deformation) may be greater or less than R. We have two situations to consider: $R >$ initial R_c and $R <$ initial R_c. Now, the rate of rotation can be zero only if $(B^2 - AC) \geq 0$. If $(B^2 - AC) < 0$, the rate of rotation cannot be zero. If $R >$ initial R_c, initial $(B^2 - AC) > 0$. If $R <$ initial R_c, initial $(B^2 - AC) < 0$. The different ways in which the rotation, either forward or backward, depends on

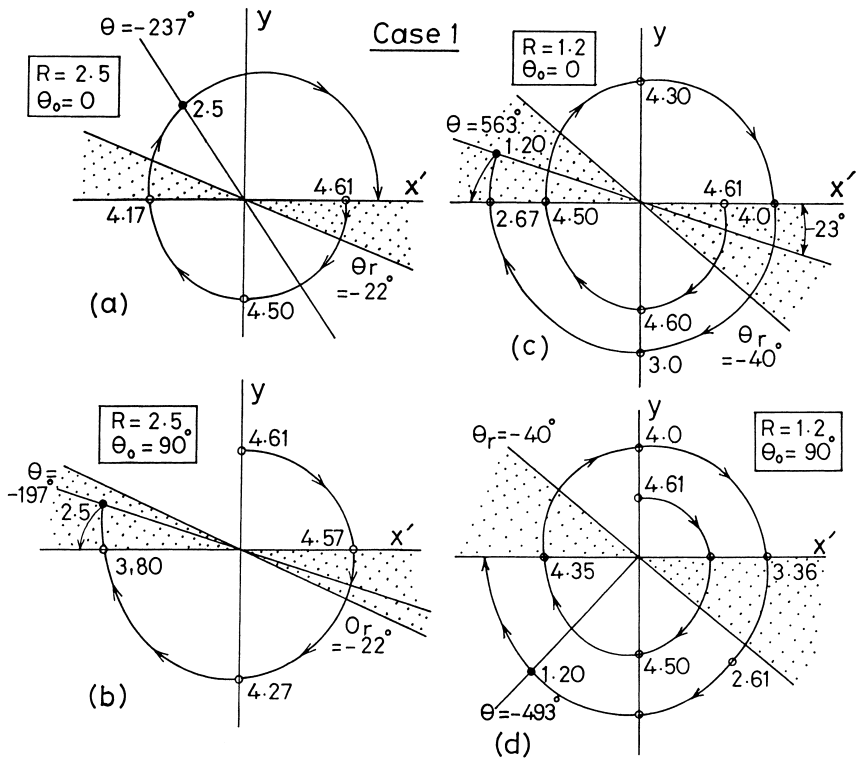

Fig. 7. Representation of change in θ and R_c with progressive deformation for case 1, with $\alpha_o = 5°$. The orientation (θ) of the E_2 axis with reference to the x' axis is obtained by joining the origin with a point lying on the spiral curve. (a) For $\theta_o = 0$, $R = 2.5$. The dotted angular domain is the range of orientation within which backward rotation is possible. At the start of deformation $R_c = 4.61$. With progressive deformation R_c decreases. $R_c = 2.5$ when the inclusion has rotated forward through an angle of $-237°$. Since the inclusion at this orientation lies outside the range of backward rotation, it rotates forward and is stabilised at $\theta = -360°$. (b) If $R = 2.5$ and $\theta_o = 90°$, the value of R_c equals 2.5 when $\theta = -197°$. The E_2 axis of the inclusion at this stage lies within the range of backward rotation. It rotates backward to be stabilised at $\theta = -180°$. (c) Rotation of inclusion with $R = 1.2$ and $\theta_o = 0$. (d) Rotation of inclusion with $R = 1.2$ and $\theta_o = 90°$. The total rotation is 630°.

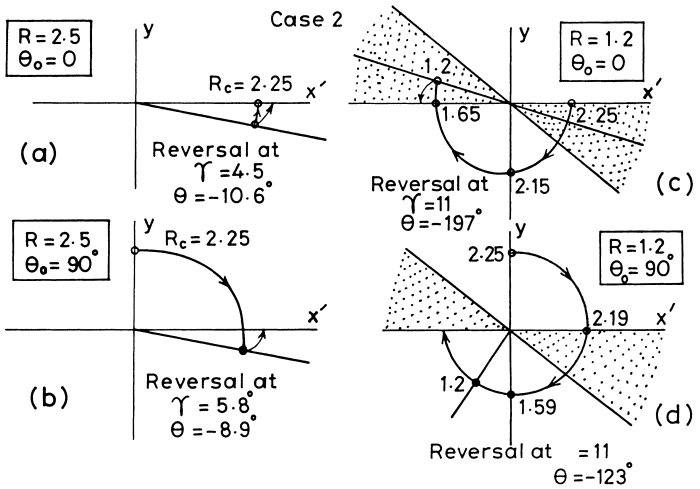

Fig. 8. Rotation of inclusions in case 2. In this case the initial $R_c = 2.25$. (a) Rotation for $R = 2.5$, $\theta_o = 0$. Since $R >$ initial R_c, R_c cannot be equal to R at any stage of progressive deformation. The inclusion rotates forward through an angle of $-10.6°$, and then rotates backward to be stabilised at $\theta = 0$. See also Fig. 9a. (b) Rotation for $R = 2.5$, $\theta_o = 90°$. The inclusion rotates forward through an angle of $-98.9°$ and then rotates backward through 8.9°, to be stabilised at $\theta = 0$. See also Fig. 9a. (c) Rotation for $R = 1.2$, $\theta_o = 0$. In this case, $R < R_c$. With progressive deformation R_c decreases. $R_c = R = 1.2$ at $\theta = -197°$. Since this orientation is within the range of backward rotation, the inclusion rotates backward through an angle of 17° to be stabilised at $\theta = -180°$. See also Fig. 9b. (d) Rotation for $R = 1.2$, $\theta_o = 90°$. $R_c = R$ when the inclusion has rotated to an orientation of $\theta = -123°$. Since this orientation is outside the range of backward rotation (dotted area) the inclusion rotates forward till it is stabilised at $\theta = -180°$.

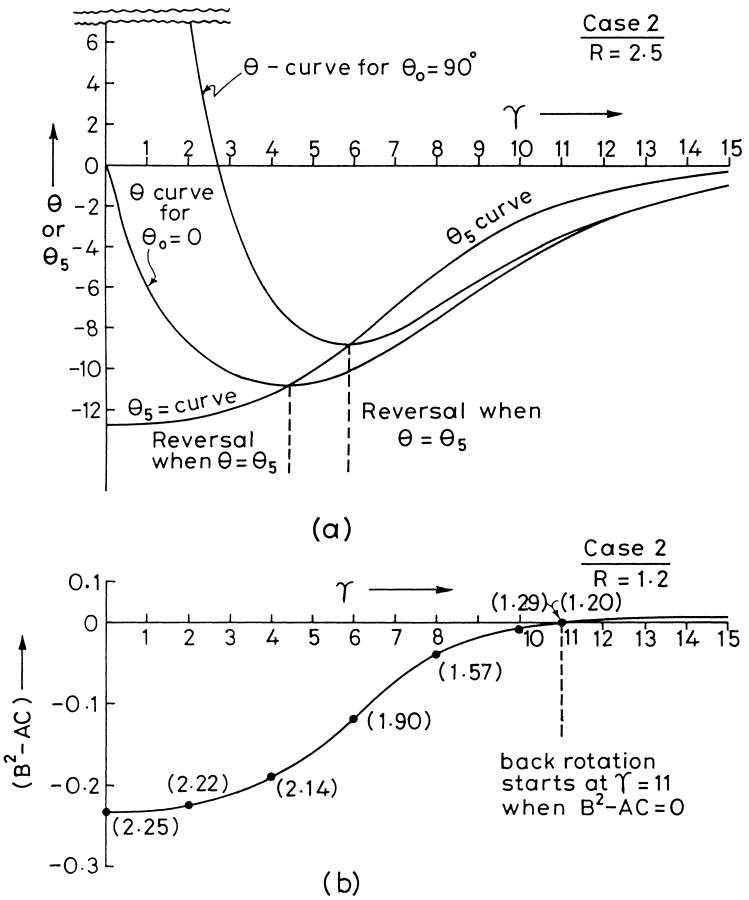

Fig. 9. (a) Change in θ_5 and θ with progressive deformation for case 2, with $R = 2.5$, $\theta_o = 0$ and $\theta_o = 90°$. Reversal in the sense of rotation occurs at a stage of deformation when the θ_5-curve intersects the θ-curve. At this stage, the rate of rotation is zero, i.e. each of the θ-curves shows a minimum, with $d\theta/d\gamma = 0$. (b) Change in the value of $(B^2 - AC)$ with progressive deformation for case 2, with $R = 1.2$, $\theta_o = 0$. Since initial R_c is $= 2.25$ and is greater than R, the initial value of $(B^2 - AC) < 0$. Hence, θ_5 given by Eq. (10) does not have a real value. With progressive deformation the algebraic value of $(B^2 - AC)$ increases. Reversal in the sense of rotation occurs when $(B^2 - AC) = 0$. At this stage of deformation $R_c = R = 1.2$. The figures in parentheses are values of R_c.

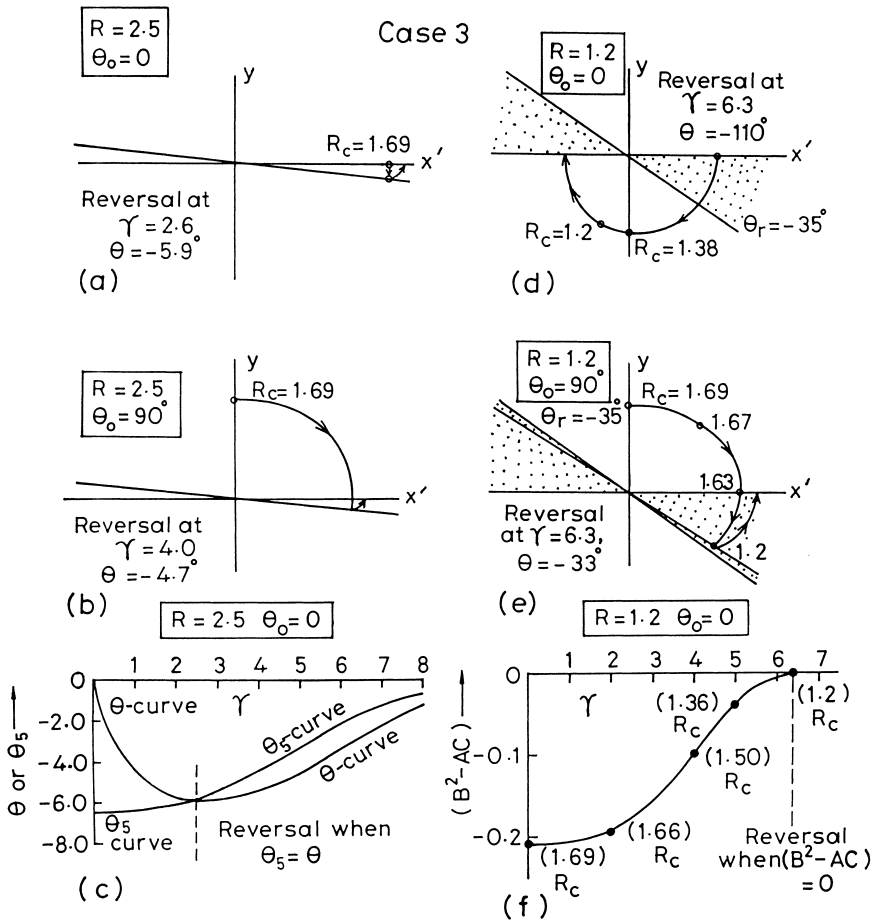

Fig. 10. Rotation of inclusions in case 3. In this case $R_c = 1.69$. (a) $R = 2.5$, $\theta_o = 0$. The inclusion rotates forward through an angle of 5.9° and then rotates backward through the same angle, to be stabilised at $\theta = 0$. (b) $R = 2.5$, $\theta_o = 90°$. The inclusion rotates forward through an angle of −94.7° and then rotates backward through 4.7°, to be stabilised at $\theta = 0$. (c) For $R = 2.5$, $R > R_c = 1.69$. The figure shows the change in θ and θ_5 with progressive deformation. (d) $R = 1.2$, $\theta_o = 0$. In this case, $R <$ initial R_c. The range of backward rotation is −35° (dotted angular domain). (e) $R = 1.2$, $\theta_o = 90°$. The inclusion rotates forward at first. R_c becomes equal to R when $\theta = -33°$. Since this orientation is within the range of backward rotation, the inclusion rotates backward through an angle of 33° and is stabilised at $\theta = 0$. (f) Since $R = 1.2 < R_c$, $(B^2 - AC)$ is negative at the initial stages. $(B_2 - AC) = 0$ and $R_c = R = 1.2$ at $\gamma = 6.3$. This is the stage of reversal of the sense of rotation.

R_c and on $(B^2 - AC)$ are shown for the four cases in Figs. 7–11.

5.2. $R >$ initial R_c

Let us first consider the situation in which $R >$ initial R_c and the initial value of $(B^2 - AC) > 0$. In this situation, the inclusion will rotate forward in the initial stages. With progressive deformation α, given by Eq. (13), will change (Fig. 6a), and hence, A, B and C, given by Eq. (12), will change. Consequently, θ_5 given by Eq. (16) and R_c given by Eq. (15) continuously change. Since R_c decreases with progressive deformation, R will always be greater than R_c, and $(B^2 - AC)$ will always remain positive. The rate of rotation will be zero when $\theta = \theta_5$. If we plot the graphs of θ and θ_5 against γ, the rate of rotation $d\theta/d\gamma$ will be zero for that value of γ at which the θ_5-curve crosses the θ-curve (Figs. 9a and 10c). Beyond this stage of deformation the rate of rotation will change sign, i.e. rotation of the inclusion will be in the backward sense. The inclusion will tend to be stabilised as θ approaches 0 or 180°. It should be noted that $\dot{\theta}/\dot{\gamma} = 0$ at $\theta = \theta_5$, but unlike the special case of $\alpha = 0$, θ_5 does not give the stable orientation of the inclusion.

As an example, let us consider a specific case (case 2) with $a = 0.5$, $b = -0.6$, $c = 0.1$. Let $R = 2.5$. Since the initial value of $R_c = 2.25$, $R >$ initial R_c. If the initial orientation $\theta_o = 0$, the θ_5-curve will intersect the θ-curve (Fig. 9a) at $\gamma = 4.5$ and $\theta = \theta_5 = -10.6°$. The inclusion will rotate forward through an angle of −10.6° and will then rotate backward. If the deformation continues, the inclusion will tend to be stabilised at $\theta = 0°$ (Fig. 8a). If the initial orientation of the inclusion was $\theta_o = 90°$ (Figs. 8b and 9a), the inclusion would rotate forward through an angle of −98.9°, and would then rotate backward with continued deformation through an angle of 8.9°, to be stabilised at $\theta = 0°$.

As a second example (Fig. 10a and c), consider the case (case 3) with $a = 0.8$, $b = -1.0$, $c = 0.2$. In this case

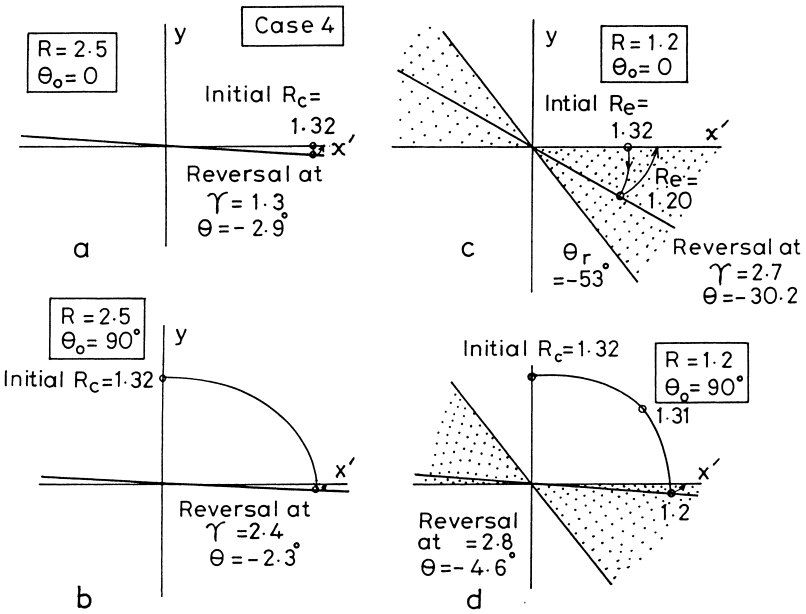

Fig. 11. Rotation of inclusions in case 4. In this case the initial $R_c = 1.32$. (a) $R = 2.5$, $\theta_o = 0$. $R_c \neq R$ at any stage of deformation. The inclusion rotates forward through an angle of $-2.9°$ and then rotates backward through the same angle and is stabilised at $\theta = 0$. (b) $R = 2.5$, $\theta_o = 90°$. The inclusion rotates through an angle of $-92.3°$ and then rotates backward by 2.3° and attains the stable orientation at $\theta = 0$. (c) $R = 1.2$, $\theta_o = 0$. In this case $R < R_c$. With progressive deformation $R_c = R = 1.2$ when $\theta = -30.2°$. Since this orientation is within the range of backward rotation (dotted) the inclusion rotates backward and is stabilised at $\theta = 0$. (d) $R = 1.2$, $\theta_o = 90°$. The inclusion rotates forward till $R_c = R$ when $\theta = -94.6°$. From this stage onward the inclusion rotates backward to be stabilised at $\theta = 0$.

$R_c = 1.69$. Let $R = 2.5$, so that $R > R_c$. If $\theta_o = 0$, the inclusion will rotate forward till $\theta = \theta_5 = -5.9°$. At this stage ($\gamma = 2.6$) the rate of rotation of the inclusion will be momentarily zero. If the deformation continues, the inclusion will rotate backward through an angle of 5.9° and will be stabilised at $\theta = 0$.

5.3. $R <$ initial R_c; the angular range of backward rotation

If $R <$ initial R_c, $(B^2 - AC) < 0$. Consequently, there is no real value of θ_5 (Eq. (16)), and the inclusion rotates forward. However, with progressive deformation, the algebraic value of $(B^2 - AC)$ increases and the value of R_c decreases. At a certain stage of deformation $(B^2 - AC)$ becomes zero (Figs. 9b and 10f). At this stage, $R_c = R$. Backward rotation may take place if deformation continues beyond this stage. But backward rotation can occur only if, at this stage of deformation, when $R_c = R$, the orientation (θ) of the inclusion lies within a certain range, namely, the angular range of backward rotation. This range is given by the angle between the x' axis ($\theta = 0$ or 180°) and a line making an angle θ_r with it, where θ_r is always negative. θ_r is determined in the following way. The value of α at which $R_c = R$ is first determined. A, B, C, as given by Eq. (12) are determined with this value of α. Then:

$$\theta_r = -B/A \tag{17}$$

At this stage of deformation, $(B^2 - AC) = 0$.

Thus, for example, let us consider case 2, with $a = 0.5$, $b = -.6$, $c = 0.1$, and with $\theta_o = 0$ and $R = 1.2$ (Figs. 8c and 9b). At the beginning of deformation, $R_c = 2.25$. Since $R <$ initial R_c, and $(B^2 - AC) < 0$, the rate of rotation cannot be zero at any value of θ. With progressive deformation the algebraic value of $(B^2 - AC)$ increases and R_c decreases. At that stage of deformation when $\gamma = 11$, $(B^2 - AC) = 0$. α can then be determined for this stage of deformation, and from Eqs. (12) and (17) it is found that $\theta_r = -40°$.

We may have two situations depending on the initial orientation θ_o. Thus, for the same example, if $\theta_o = 0$, $R = 1.2$, the inclusion rotates forward. R_c becomes equal to R (1.2) when the inclusion has rotated forward (i.e. in the clockwise sense) through an angle of $-197°$, i.e. at an acute angle of $-17°$ with the x' axis. Since this orientation is within the range of backward rotation (dotted area of Fig. 8c), the inclusion rotates backward from this stage. If progressive deformation continues, the inclusion will be stabilised at $\theta = -180°$. Again, if $\theta_o = 90°$ (Fig. 8d), R_c becomes equal to R and $(B^2 - AC)$ becomes zero (Fig. 9b) at a stage of deformation when the inclusion has rotated clockwise through an angle of $-213°$, i.e. at an orientation of $\theta = -123°$. Since this orientation is outside the range of backward rotation (dotted angular domain in Fig. 8d), the inclusion will continue to rotate forward till it attains its stable orientation at $\theta = -180°$.

The maximum possible rotation of a long clast with fixed initial values of α_o and θ_o depends on the nature of bulk deformation, i.e. on the strain-rate ratios a, b and c. Among the four cases considered by us for numerical examples, the

Table 1
Maximum rotation and stable position of inclusions for four cases with $\theta_o = 0°$, $\alpha_o = 5°$

R	Cases	Maximum forward rotation (°)	Maximum backward rotation (°)	Orientation stabilised at:
1.0	Case 1: $a = 0.2$	596		
	Case 2: $a = 0.5$	225		
	Case 3: $a = 0.8$	146		
	Case 4: $a = 1.5$	86		
1.2	Case 1: $a = 0.2$	563	23	$540° = 180° \times 3$
	Case 2: $a = 0.5$	197	17	180°
	Case 3: $a = 0.8$	180	0	180°
	Case 4: $a = 1.5$	30.2	30.2	0°
1.5	Case 1: $a = 0.2$	540	0	$540° = 180° \times 3$
	Case 2: $a = 0.5$	182.6	2.6	180°
	Case 3: $a = 0.8$	29	29	0°
	Case 4: $a = 1.5$	11.5	11.5	0°
2.0	Case 1: $a = 0.2$	375	15	360°
	Case 2: $a = 0.5$	20	20	0°
	Case 3: $a = 0.8$	10	10	0°
	Case 4: $a = 1.5$	4.6	4.6	0°
2.5	Case 1: $a = 0.2$	360	0	360°
	Case 2: $a = 0.5$	10.6	10.6	0°
	Case 3: $a = 0.8$	5.9	5.9	0°
	Case 4: $a = 1.5$	2.9	2.9	0°

relative contribution of simple shearing decreases from case 1 to case 4. Table 1 shows that for any value of R, the maximum forward rotation decreases from case 1 to case 4. It also shows that, for any one of these cases, the maximum forward rotation decreases as R increases.

6. Discussion

Rotated rigid objects may give us valuable information on different aspects of the bulk deformation. Thus, for example, patterns of distorted foliation around rotated rigid objects (e.g. Ghosh and Ramberg, 1976; Ghosh, 1977; Simpson and Schmid, 1983; Passchier and Simpson, 1986; Van Den Driessche and Brun, 1987; Passchier and Trouw, 1996) have often been used to determine the sense of shear in ductile shear zones. An analysis of the stable positions of elongate rigid objects of different aspect ratios may also give us some information about the nature of bulk deformation (e.g. Simpson and De Paor, 1993, 1997). For an ellipsoidal or cylindroidal object, such analyses of the rotational history of rigid objects commonly involve the assumption that the cylinder axis or one of the principal axes of the ellipsoidal object remains parallel to the vorticity vector ($\alpha = 0$). The rotation history of rigid objects in transpressional shear zones will be quite different when $\alpha = 0$ and $\alpha \neq 0$. The major points of difference are summarised in Table 2. In numerical calculations for the case of $\alpha \neq 0$, we have taken the value of α_o as 5°. There is no significant difference in our conclusions if a somewhat smaller or larger value of α is taken. It should be noted that if $\alpha = 0$, the equations for rates of rotation and of finite

Table 2
Comparison of rotation of long clasts for $\alpha = 0$ and $\alpha \neq 0$

$\alpha = 0$	$\alpha \neq 0$
E_1 axis does not rotate.	E_1 axis rotates towards direction of maximum stretching.
Rate of rotation and finite rotation of E_2 around E_1 depends upon a single parameter $(a - b)$ of bulk deformation.	Rate of rotation and finite rotation depends on three strain-rate ratios a, b, c of which two are independent.
For known $(a - b)$ and R, $\theta'/\dot{\gamma} = 0$ at fixed orientations. $\theta'/\dot{\gamma}$ is independent of rotation history.	No fixed orientation at which $\theta'/\dot{\gamma} = 0$. It changes with progressive deformation.
For $R = 1$, $\theta'/\dot{\gamma}$ is a constant i.e. $\theta'/\dot{\gamma} = 0.5$.	For $R = 1$, $\theta'/\dot{\gamma}$ continuously decreases.
There is either forward or backward rotation. Rate of rotation does not change sign with progressive deformation.	The rotation history may involve both forward and backward rotation.
If deformation continues the total rotation is unlimited for relatively small value of R.	Total rotation is limited for all inclusions.
Stable orientation is at an angle to shear zone walls.	Stable orientation (for $R \neq 1$) is parallel to shear zone walls.
Nature of bulk deformation, $(a - b)$, may be determined from stable orientation and R.	Nature of bulk deformation cannot be determined from stable orientation.

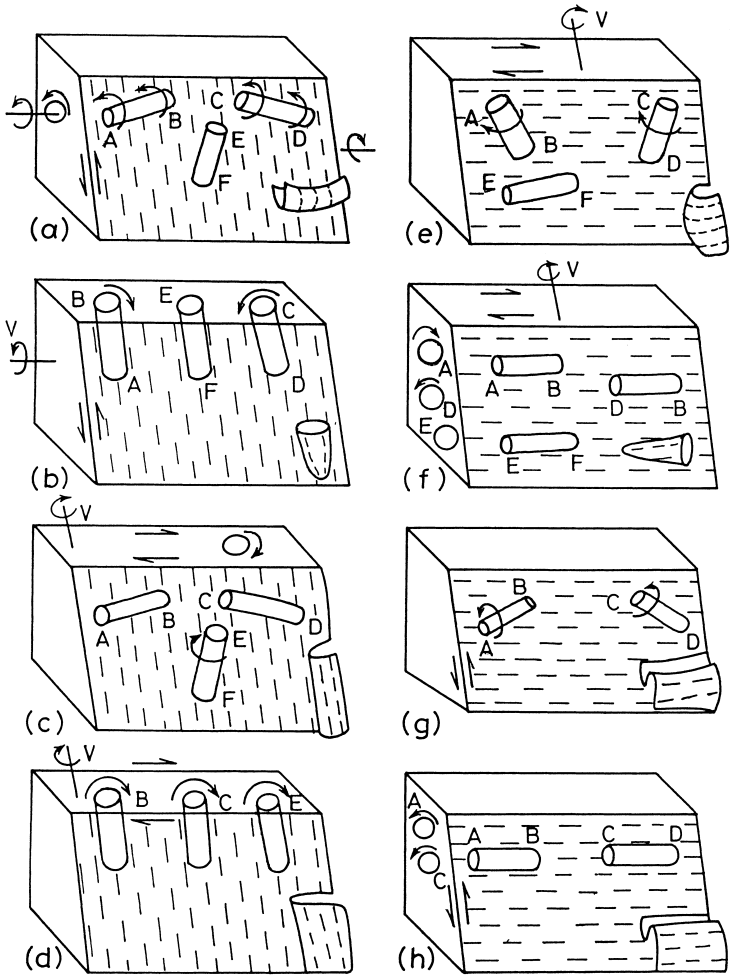

Fig. 12. (a) Shear zone with down-dip stretching lineations (dashed lines) and a dip-slip sense of shear. AB, CD and EF are long cylindrical clasts, and in lower right is a syn-thrusting fold in the initial stage of deformation. The horizontal vorticity vector V shows a sinistral sense of rotation when viewed from the left side. (b) Same type of shear zone as in (a) but after a very large deformation. (c) and (d) Initial and final stages of rotation of long clasts in a shear zone with down-dip stretching lineation (dashed lines) and dextral strike-slip shear. (e) and (f) Transpressional shear zone with subhorizontal stretching lineation and dextral strike-slip sense of shear; (e) initial and (f) final stages of deformation. (g) and (h) Initial and final stages of rotation of axes of long clasts in shear zones with subhorizontal stretching lineations and dip-slip sense of shear. At an advanced stage of deformation the cross-sectional faces of the long clasts on dip-sections show the same sense of rotation. Sheath folds are not expected in this case.

rotation of elongate inclusions, for the type of deformation considered here, are obtained by replacing the parameter s_r in the equations of Ghosh and Ramberg (1976) by the entity $\frac{1}{2}(a - b)$.

Sheath folds and segments of isoclinal folds often occur parallel to the stretching lineation in ductile shear zones. Many of these contemporary folds initiated broadly orthogonal to the shear direction and to the stretching lineation, and were rotated towards the stretching direction during ductile shearing (e.g. Bryant and Reed, 1969; Sanderson, 1973; Escher and Watterson, 1974; Rhodes and Gayer, 1977; Bell, 1978; Minnigh, 1979; Ghosh and Sengupta, 1987, 1990; Mies, 1991; Alsop and Holdsworth, 1999; Ghosh et al., 1999). Rotation of contemporary folds through a large angle is also indicated by occurrence of U-shaped lineation patterns (Ghosh and Sengupta, 1987; Ghosh et al., 1999) over hinges of transport-parallel folds. Depending upon the initial orientation (i.e. the sign of α_o), the hinge lines may rotate in both clockwise and counterclockwise sense (viewed from above in the XY plane); consequently, folds with a single sense of asymmetry, when they were more or less orthogonal to the lineation, may show S or Z asymmetry after they are rotated parallel to the lineation (Hazra, 1997; Alsop and Holdsworth, 1999). Such a rotation history of folds implies that the stretching lineation is orthogonal, or at a large angle to the vorticity vector. On the other hand, stretching lineations subparallel to the vorticity vector have been reported from a number of transpressional shear zones (e.g. Robin and Cruden, 1994; Hudleston et al., 1988; Fossen and Tikoff, 1993). Strongly rotated folds and sheath folds produced by large rotation of fold hinges are unlikely to occur in such shear zones. Sheath folds may also develop by deflection of foliation around rigid objects (Cobbold and Quinquis, 1980). However, as

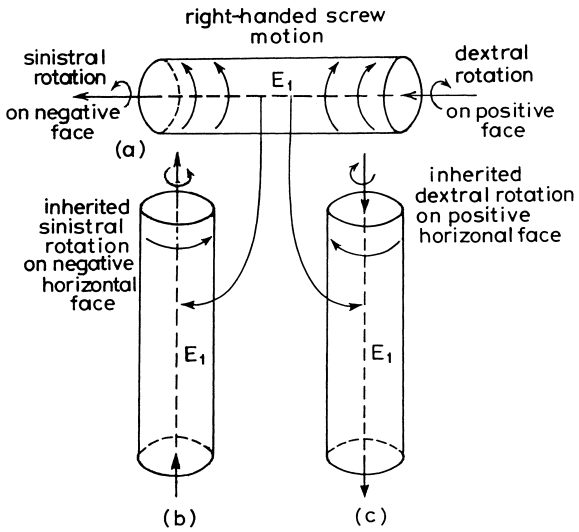

Fig. 13. Different senses of inherited rotation on the upper cross-sectional face of a cylindrical object, the axis of which has rotated clockwise or counterclockwise. The vorticity vector is horizontal. (a) In a subhorizontal position, the cylinder has the same sense of rotation as the vorticity vector, i.e. a right-handed screw motion. Let the right hand face be considered as positive (with arrow pointing along inward normal). On the positive face on the right hand side the rotation is dextral and on the left-hand side the rotation is sinistral. (b) If the cylinder axis is rotated clockwise from a subhorizontal to a subvertical position, the negative cross-sectional face with an inherited sinistral sense of rotation appears on the top horizontal surface. (c) If the cylinder axis is rotated counterclockwise, the positive cross-sectional face with dextral sense of rotation comes to the top surface.

pointed out by Platt (1983) and Mies (1991), most contemporary shear zone sheath folds are not associated with 'islands' of undeformed rocks.

If we consider the deformation within the shear zone to be a result of a combination of wall-parallel simple shearing and coaxial deformation as in Fig. 1a, we may have two situations depending on whether the direction of maximum stretching is parallel or perpendicular to the vorticity vector. Fig. 12 shows these two situations in terms of four types of transpressional ductile shear zones: (1) with a dip-slip sense of wall-parallel shear and with the direction of maximum wall-parallel stretching perpendicular to the vorticity vector (i.e. with a down-dip stretching lineation) (Fig. 12a and b); (2) with a strike-slip sense of wall-parallel shear and with the direction of maximum wall-parallel stretching parallel to the vorticity vector (i.e. with down-dip stretching lineation) (Fig. 12c and d); (3) with a strike-slip sense of wall-parallel shear and with subhorizontal stretching lineation (Fig. 12e and f); and (4) with a dip-slip sense of wall-parallel shear and with the direction of maximum wall-parallel stretching parallel to the vorticity vector (i.e. with a subhorizontal stretching lineation) (Fig. 12g and h). These four cases belong to two above-mentioned categories, with the stretching lineation perpendicular and parallel to the vorticity vector. Shear zones represented in Fig. 12 (a and b and e and f) belong to the first of these categories, whereas shear zones as in Fig. 12 (c and d and g and h) belong to the second category. Representation of the shear zones with dip-slip and strike-slip senses as in Fig. 12 is merely for the sake of convenience of description. The analysis is also valid for oblique-slip shear zones obtained by a rigid body rotation of the co-ordinate axes.

When the stretching lineation is parallel to the vorticity vector as in Fig. 12 (c and d and g and h), the folds initiate subparallel to the stretching lineation, and undergo little or no rotation. The long tectonic clasts that were initially parallel to the fold hinge lines will remain parallel to the vorticity vector. Rotation of the E_2 axis of these long clasts may then take place around the E_1 axis that maintains a more or less constant orientation during the major part of deformation. When the stretching lineation is at a right angle the vorticity vector as in Fig. 12 (a and b or e and f), fold hinge lines and the E_1 axes of long clasts, such as boudin axes and rodding, will initially make a large angle with the stretching lineation. Since this orientation is unstable they will rotate towards the direction of stretching and will become subparallel to it at an advanced stage of deformation. Sheath folds are likely to be associated with such strongly rotated long clasts.

One of the most important geological consequences of rotation of clasts in transpressional ductile shear zones, where $\alpha \neq 0$, is that, depending upon its initial orientation α_o, the longest axis (E_1) of the clast may rotate either in clockwise or counterclockwise sense, in a plane parallel to the shear zone wall. The rotation of the E_2 axis around the E_1 axis will, however, be always compatible with the sense of vorticity. To describe the sense of rotation around the E_1 axis in terms of clockwise and counterclockwise sense (or dextral and sinistral), we need to specify the face on which the observation is made. The sense of rotation around the subhorizontal E_1 axis of a cylindrical clast in the initial stages of deformation in, for example, a dip-slip shear zone with down-dip stretching lineation, will be clockwise when a cross-sectional face is seen from the right hand side (Figs. 12a and 13a). Let the normal of this face be considered as positive (with inward pointing arrow in Fig. 13a). The opposite face will be considered as negative (with outward pointing arrow for the normal). If after a large deformation the cylinder axis rotates counterclockwise, and becomes subparallel to the down-dip stretching lineation, the positive cross-sectional face of the cylindrical object will appear on the horizontal outcrop face (Fig. 13c). Since this face is parallel to the vorticity vector (Fig. 12b), the component of shear on this outcrop face is zero. Yet, the distorted foliation pattern around the cross-section of the clast will show an inherited dextral asymmetry and an apparent dextral sense of shear. If, however, the sign of α_o was such that the E_1 axis rotated in a clockwise sense and became subparallel to the down-dip direction of the shear zone, the negative cross-sectional face would appear on the horizontal upper surface (Figs. 12b and 13b). The asymmetry of the distorted foliation around the cross-section of the reoriented clast will then show an inherited sinistral shear. In a shear zone in which the initial α_o of the different clasts were both positive

and negative, the distorted patterns of foliation around the rotated clasts may show both dextral and sinistral senses of shear on an outcrop face that is parallel to the vorticity vector, although on this face the component of simple shearing is zero. A similar situation may also arise in strike-slip shear zones in which the stretching lineation is subhorizontal. Thus, among the four types of shear zones shown in Fig. 12, those that have the stretching lineation at a right angle to the vorticity vector (Fig. 12b and f) will show opposite senses of inherited rotation of the E_2 axis around the E_1 axis of long clasts on an outcrop face at a right angle to stretching lineation. In contrast, shear zones in which the stretching lineation is parallel to the vorticity vector will always show the same sense of rotation around the E_1 axis on a surface at a right angle to the stretching lineation (Fig. 12c and h).

The sense of shear, implied by the sense of asymmetry of deformed foliations around rotated clasts, is generally determined from two-dimensional observations, either in oriented thin sections or in sections of clasts in outcrop faces. Unless the shear sense is independently known from other shear criteria, we cannot be sure whether the asymmetry in a lineation-parallel (foliation-normal) or a lineation-normal section would give us the true sense of shear. If the stretching lineation is parallel to the vorticity vector, the shear direction can be determined from monoclinic fabrics on lineation-normal sections; the lineation parallel section would show an orthorhombic fabric. If the stretching lineation is orthogonal to the vorticity vector, monoclinic and orthorhombic fabrics will appear in lineation-parallel and lineation-normal sections, respectively, provided a principal axis of non-spherical clasts is subparallel to the vorticity vector. This can no doubt be checked by determining the three-dimensional forms of the clasts or simply from their shapes in foliation-parallel sections. If, as in the model given above, the long axes of the clasts have undergone large rotation within the foliation plane, monoclinic rolling fabrics may appear in both lineation-parallel and lineation-normal sections. The lineation-normal sections may show opposite senses of asymmetry of the rolling structures if the initial angle α_o was both positive and negative for different clasts. The true shear sense can then be determined from lineation-parallel sections.

Examples of such opposite senses of rotation around the long axis of cylindrical clasts are frequently found on horizontal outcrop-faces in the Phulad shear zone of Rajasthan, India. This shear zone (Ghosh et al., 1999) has a thrusting sense of movement, a subhorizontal vorticity vector and a down-dip stretching lineation, with profuse development of sheath folds with their long arms subparallel to the lineation. Opposite senses of rotation of hinge lines of asymmetric folds in the shear zone has given rise to opposite senses of asymmetry on the horizontal profile planes of steeply plunging hinge lines of arms of sheath folds (Hazra, 1997). A detailed analysis of the rotation history of long clasts of the Phulad shear zone will be presented in a later publication.

We may also consider the possibility that the angles (α_o) for all long clasts in a shear zone domain had the same sign, and consequently the E_1 axis of all clasts rotated in the same sense within the foliation. Each of the lineation-parallel and lineation-normal sections would then show a single sense of asymmetry of the structures. The rolling structures associated with only the spherical clasts will give the true sense of shear. A similar case of single sense of rotation of fold hinges towards the stretching direction was reported by Alsop (1992) from the Ballybofey Nappe of northwest Ireland.

The model presented here is applicable to transpressional shear zones, which contain long tectonic clasts, and in which the stretching lineation is either parallel or perpendicular to the transport direction. It is not a general model; it does not consider the rotation of an ellipsoidal inclusion with axes initially oblique to all the co-ordinate axes (e.g. Freeman, 1985; Arbaret et al., 2001). Neither is it applicable to all types of transpressional shear zones (e.g. Tikoff and Fossen, 1993; Robin and Cruden, 1994; Tikoff and Greene, 1997; Jones and Holdsworth, 1998), with more complex relations between the stretching lineation and the vorticity vector.

Acknowledgements

This work was made possible by the financial support of the Indian National Science Academy and the Council of Scientific and Industrial Research. We thank J. Hippert, N. Mancktelow and F. Marques for their critical comments and suggestions.

References

Alsop, G.I., 1992. Progressive deformation and the rotation of contemporary fold axes in the Ballybofey Nappe, north-west Ireland. Geological Journal 27, 271–283.

Alsop, G.I., Holdsworth, R.E., 1999. Vergence and facing patterns in large-scale sheath folds. Journal of Structural Geology 21, 1335–1349.

Arbaret, L., Mancktelow, N.S., Burg, J.-P., 2001. Effect of shape and orientation on rigid particle rotation and matrix deformation in simple shear flow. Journal of Structural Geology 23, 113–125.

Bell, T.H., 1978. Progressive deformation and reorientation of fold axes in a ductile mylonite zone: the Woodroffe thrust. Tectonophysics 44, 285–320.

Bryant, B., Reed, J.C., 1969. Significance of lineation and minor folds near major thrust faults in the southern Appalachian and the British and Norwegian Caledonides. Geological Magazine 106, 412–429.

Cobbold, P.R., Quinquis, H., 1980. Development of sheath folds in shear regimes. Journal of Structural Geology 2, 119–126.

Escher, A., Watterson, J., 1974. Stretching fabrics, folds and crustal shortening. Tectonophysics 22, 223–231.

Fossen, H., Tikoff, B., 1993. The deformation matrix for simultaneous

simple shearing, pure shearing and volume change, and its application to transpression–transtension. Journal of Structural Geology 15, 413–422.

Freeman, B., 1985. The motion of rigid particles in slow flows. Tectonophysics 34, 163–183.

Ghosh, S.K., 1977. Drag patterns of planar structures around rigid inclusions. In: Saxena, S.K., Bhattacharji, S. (Eds.), Energetics of Geological Processes, Springer-Verlag, New York, pp. 94–120.

Ghosh, S.K., 2001. Types of transpressional and transtensional deformation. In: Koyi, H.A., Mancktelow, N.S. (Eds.), Tectonic Modeling: A Volume in Honor of Hans Ramberg. Geological Society of America Memoir 193, pp. 1–20.

Ghosh, S.K., Ramberg, H., 1976. Reorientation of inclusions by combination of pure shear and simple shear. Tectonophysics 34, 1–70.

Ghosh, S.K., Sengupta, S., 1973. Compression and simple shear of test models with rigid and deformable inclusions. Tectonophysics 17, 133–175.

Ghosh, S.K., Sengupta, S., 1987. Progressive evolution of structures in a ductile shear zone. Journal of Structural Geology 9, 277–288.

Ghosh, S.K., Sengupta, S., 1990. Singhbhum Shear Zone: structural transition and a kinematic model. Proceedings of the Indian Academy of Sciences (Earth and Planetary Sciences) 99, 229–247.

Ghosh, S.K., Hazra, S., Sengupta, S., 1999. Planar, non-planar and refolded sheath folds in Phulad shear zone, Rajasthan, India. Journal of Structural Geology 21, 1715–1729.

Hazra, S., 1997. Sense of fold asymmetry in single phase and superposed folding. In: Sengupta, S., (Ed.), Evolution of Geological Structures in Micro- to Macro-scales, Chapman and Hall, pp. 397–409.

Hudleston, P.J., Schultz-Ela, D., Southwick, D.L., 1988. Transpression in Archean Greenstone belt, Minnesota. Canadian Journal of Earth Science 25, 1060–1068.

Jones, R.R., Holdsworth, R.E., 1998. Oblique simple shear in transpression zones. In: Holdsworth, R.E., Strachan, R.A, Dewey, J.F. (Eds.), Continental Transpressional and Transtensional Tectonics. Geological Society, London, Special Publications 135, pp. 35–40.

Mies, J.W., 1991. Planar dispersion of folds in ductile shear zones and kinematic interpretation of fold-hinge girdles. Journal of Structural Geology 13, 281–297.

Minnigh, L.D., 1979. Structural analysis of sheath folds in a meta-chert from the western Italian Alps. Journal of Structural Geology 1, 275–282.

Passchier, C.W., 1987. Stable positions of rigid objects in noncoaxial flow—a study in vorticity analysis. Journal of Structural Geology 9, 679–690.

Passchier, C.W., Simpson, C., 1986. Porphyroclast systems as kinematic indicators. Journal of Structural Geology 8, 831–843.

Passchier, C.W., Trouw, R.A.J., 1996. Microtectonics, Springer, Berlin.

Platt, J.P., 1983. Progressive refolding in ductile shear zones. Journal of Structural Geology 5, 619–622.

Rhodes, S., Gayer, R.A., 1977. Non-cylindrical folds, linear structures in the X direction and mylonite developed during translation of the Caledonian Kalak Nappe Complex of Finnmark. Geological Magazine 114, 329–408.

Robin, P.Y., Cruden, A.R., 1994. Strain and vorticity patterns in ideally ductile transpressional zones. Journal of Structural Geology 16, 447–466.

Sanderson, D.J., 1973. The development of fold axis oblique to the regional trend. Tectonophysics 16, 55–70.

Simpson, C., De Paor, D.G., 1993. Strain and kinematic analysis in general shear zones. Journal of Structural Geology 15, 1–20.

Simpson, C., De Paor, D.G., 1997. Practical analysis of general shear zones using the porphyroclast hyperbolic distribution method: an example from the Scandinavian Caledonides. In: Sengupta, S., (Ed.), Evolution of Geological Structures in Micro- to Macro-scales, Chapman and Hall, pp. 169–184.

Simpson, C., Schmid, S.M., 1983. An evaluation of criteria to deduce the sense of movement in sheared rocks. Geological Society of America Bulletin 94, 1281–1288.

Tikoff, B., Fossen, H., 1993. Simultaneous pure and simple shear: the unified deformation matrix. Tectonophysics 217, 267–283.

Tikoff, B., Greene, D., 1997. Stretching lineations in transpressional shear zones: an example from the Sierra Nevada Batholiths, California. Journal of Structural Geology 19, 29–39.

Van Den Driessche, J., Brun, J.-P., 1987. Rolling structures at large shear strains. Journal of Structural Geology 9, 691–704.